

An ARPES spectral function analysis of the electron doped cuprate $\text{Nd}_{1.85}\text{Ce}_{0.15}\text{CuO}_4$

N.P. Armitage^{1,2,3}, D.H. Lu³, C. Kim³, A. Damascelli^{3,4}, K.M. Shen^{3,4}, F. Ronning^{2,3}, D.L. Feng^{2,3}, P. Bogdanov^{3,4}, X.J. Zhou^{3,5}, W.L. Yang⁵, Z. Hussain⁵, P. K. Mang^{3,4}, N. Kaneko^{3,4}, M. Greven^{3,4}, Y. Onose⁶, Y. Taguchi⁶, Y. Tokura⁶, and Z.-X. Shen^{2,3,4}

¹*Department of Physics and Astronomy, University of California, Los Angeles, CA 90095*

²*Department of Physics, Stanford University, Stanford, CA 94305*

³*Stanford Synchrotron Radiation Laboratory, Stanford University, Stanford, CA 94305*

⁴*Department of Applied Physics, Stanford University, Stanford, CA 94305*

⁵*Advanced Light Source, Lawrence Berkeley National Laboratory, Berkeley, CA 94720*

⁶*Department of Applied Physics, The University of Tokyo, Tokyo 113-8656, Japan*

(February 7, 2020)

Using methods made possible by recent advances in photoemission technology, we perform an in-depth line shape analysis of the ARPES spectra of the electron doped (*n*-type) cuprate superconductor $\text{Nd}_{1.85}\text{Ce}_{0.15}\text{CuO}_4$. Unlike the *p*-type materials, we observe weak mass renormalizations near 50-70 meV. This may be indicative of either weaker electron-phonon coupling or due to the masking effects of other interactions that make the electron-phonon coupling harder to detect. This latter scenario may suggest limitations of the spectral function analysis in extracting electronic self-energies when some of the interactions are highly momentum dependent.

PACS numbers: 79.60.Bm, 73.20.Dx, 74.72.-h

I. INTRODUCTION

Angle resolved photoemission spectroscopy (ARPES) is one of the most direct probes of the electronic structure of solids. In recent years, with the advent of *Scienta* analyzers and high-flux beamlines, a new era of photoemission lineshape analysis has been ushered in [1]. The advances offer unprecedentedly high energy and momentum resolution, as well as the ability to do simultaneous parallel angle scanning and thereby generate direct 2D $E-\vec{k}$ images of ARPES spectral functions. Whereas, ARPES data have been traditionally displayed in terms of energy distribution curves (EDCs) where the photoemission intensity is plotted as a function of energy at specific angles, now ARPES data can be represented in terms of these detailed false intensity plots and in analogy with EDCs, complementary momentum distribution curves (MDCs) can be generated. Such advances are making new analysis methods possible, where one is able to bring to bear the considerable mathematical machinery of many-body physics for intuition and interpretation.

Within the sudden approximation, ARPES measures the single-particle spectral function $A(\vec{k}, \omega)$ [1,2]. Assuming that the material has well-defined electronic excitations, the single particle spectral function can be represented compactly in terms of a complex self-energy $\Sigma = \Sigma' + i\Sigma''$ as

$$A(\vec{k}, \omega) = \frac{1}{\pi} \frac{\Sigma''(\vec{k}, \omega)}{[\omega - \epsilon_{\vec{k}} - \Sigma'(\vec{k}, \omega)]^2 + [\Sigma''(\vec{k}, \omega)]^2} \quad (1)$$

In momentum regions where $\Sigma(\vec{k}, \omega)$ is a weak function of \vec{k} and the bare dispersion can be linearized as

$\epsilon_{\vec{k}} = \vec{v}_F^0 \cdot (\vec{k} - \vec{k}_F)$ (where \vec{v}_F^0 is the bare band velocity) $A(\vec{k}, \omega)$ at constant ω can be put in the form of a Lorentzian centered at $\omega/\vec{v}_F^0 + k_F - \Sigma'(\vec{k}, \omega)/\vec{v}_F^0$ with width $\Sigma''(\vec{k}, \omega)/\vec{v}_F^0$.

We should note that this analysis is predicated on the fact that it is physically reasonable to express interaction effects as *electronic* self-energies. In this sense, the marginal Fermi liquid phenomenology [3] may represent a “worst case” scenario in assigning physical meaning to such self-energies. If in fact the cuprates are non-Fermi liquids in the sense that the fundamental excitations have integrity that are distinct from electrons, this analysis may not be valid. Indeed in such a case or in any case where the MDCs are not well represented as Lorentzians, this analysis will cause an inaccurate and unphysical parameterization of the spectra.

Fits to such MDCs gives one, in principle, not only a measure of $\Sigma''(\vec{k}, \omega)$, but also a more accurate parameterization of the renormalized dispersion in the case of a rapidly changing $\Sigma'(\vec{k}, \omega)$. Such an analysis allows one to probe the dominant kinds of electron-electron interactions as well as for signatures of electronic interaction with bosonic modes.

Such studies are an area of much current focus in the ARPES community with, for instance, the observance of bosonic effects in the ARPES spectra of strongly coupled electron-phonon systems (Be and Mo) [4–6]. The case of the Be (0001) surface state is a particularly beautiful example of this kind of treatment [4,5]. Here, a two peak structure in the EDC is indicative of strong electron-phonon coupling. In their analysis, LaShell *et al.* constructed MDCs and showed from a lineshape analysis

how one could reasonably extract parameters like the Debye energy (ω_D) and the dimensionless electron-phonon coupling parameter (λ) [5].

Recently, certain similar features have been found in the low-energy ARPES spectra of a number of high-temperature hole doped cuprate superconductors. A mass renormalization, or “kink”, in the dispersion has been found ubiquitously in the *p*-type materials (at ≈ 70 meV) [7,8]; its origin is a matter of much current debate. Some groups have pointed to a many-body electronic source [9–11], that is perhaps related to the magnetic resonance mode discovered *via* neutron scattering. However, this assignment has been disputed on the grounds that the resonant mode has insufficient spectral weight to cause the observed effect with general estimates for its coupling strength [12]. Others have argued that the kink’s presence above T_c and its universality between material classes demonstrates a phononic origin and indicates the strong (and largely neglected) role that lattice effects have on the low-energy physics [8].

Such studies are important, as one of the problems in the field of high- T_c superconductivity has been an inability to distinguish between similar symptoms of ultimately very different competing effects. Although in principle it is straightforward with the above analysis to extract the electronic self-energy from ARPES spectra, it is not as obvious how to assign parts of the self-energy to different sources. For instance, is the underlying phenomenon that causes the kink, the same one that causes the pseudogap in the underdoped materials, or are multiple effects playing a role? Moreover, there have even been reports that distinguish between different types of kinks at the $(\pi, 0)$ position [11]. As it is a tall order to be able to distinguish between similar manifestations of the various phononic, antiferromagnetic, charge order, stripe, and structural effects (not to mention the possibility of hidden orders [13]) that may exist in the cuprates, the best prescription seems to be the one followed primarily in the literature thus far; isolate a feature (the kink for instance) in a certain region of the Brillouin zone (BZ), or part of the phase diagram where other effects are minimized, and follow it into regions where it may not be unambiguously identified.

Such problems may be particularly acute in the electron doped system $\text{Nd}_{2-x}\text{Ce}_x\text{CuO}_4$ [14]. In previous ARPES work on the “optimally-doped” ($x = 0.15$) system, high-energy pseudogap effects similar to those in the underdoped *p*-type compounds were observed [15,16]. However, unlike in the *p*-types, these regions of maximum pseudogap were not at the Fermi surface (FS) near $(\pi, 0)$ (the maximum of the $d_{x^2-y^2}$ functional form), but instead at “hot-spots” at the intersection of the FS with the antiferromagnetic Brillouin zone (AFBZ) boundary [15]. This, along with the fact that these highest T_c samples ($x = 0.15$) in the $\text{Nd}_{2-x}\text{Ce}_x\text{CuO}_4$ system are in very close proximity to the antiferromagnetic phase (the two ground

states are separated by 1% neodymium concentration), led to the conclusion that this high-energy pseudogap was due to the lingering effects of antiferromagnetic (or similar) order with characteristic wavevector (π, π) [15].

As the signatures of boson-electron interactions are somewhat generic, it may be difficult to distinguish interactions with different types of modes if the regions of the BZ, where such effects are strongest, overlap. In this way, if the kink in the hole doped materials derives from a coupling to phonons then the residual effects of magnetism in extended regions of the BZ in the electron doped material may make its unambiguous identification in the self-energy difficult. This may be contrasted with the *p*-type compounds where large pseudogap effects are found only in underdoped samples and are largely confined to regions of the BZ near $(\pi, 0)$. In the context of Eq. 1, this may raise the question of the \vec{k} -independence of the self-energy implied in the analysis of our earlier study and may underlie some of the puzzling results [8].

Keeping the above considerations in mind, we present a ARPES lineshape analysis of the electron doped (*n*-type) cuprate superconductor $\text{Nd}_{1.85}\text{Ce}_{0.15}\text{CuO}_4$. We use essentially same methodologies that have been employed on the *p*-type compounds as we believe a direct comparison has utility despite the fact that there may be possible complications. We concentrate on those regions of the BZ away from the “hot-spots” i.e. the Γ to (π, π) FS crossing and the $(\pi, 0)$ to (π, π) FS crossing. The situation of the *n*-type material near optimal doping is very different from its *p*-type counterpart, and extraction of the electron-boson interaction parameters may not be as straightforward. We find that there is essentially no kink along the zone diagonal, in contrast to the *p*-type materials where this is the region of the BZ where it can be most unambiguously identified. In the $(\pi, 0)$ to (π, π) direction, a very weak kink in the quasiparticle dispersion can be found. However, it is not straightforward to identify this effect with phonons as competing effects cannot be unambiguously separated in this region of the BZ. Despite not observing a mass renormalization along the zone diagonal, a very slight drop in the scattering rate may be observed in this direction. No such drop in the scattering rate is observed near the $(\pi, 0)$ to (π, π) FS crossing.

At face value, these are contradictory results for the dispersion and scattering rate, as the data from the two directions are not consistent with the Kramers-Kronig relations and imply that one may not be able to analyze the data in a simple fashion at least quantitatively. This may be caused by a stronger \vec{k} -dependence of the self-energy in these materials. As it is reasonable that this class of many-body effects along the nodal direction in the *p*-type compounds can be identified with effects of phonons, at the qualitative level the lack of a kink and weak drop in the scattering rate along the same

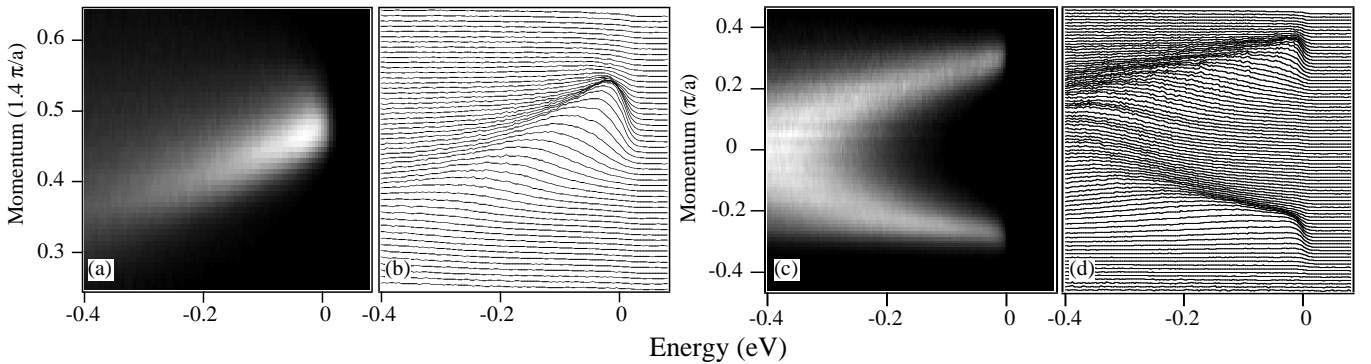


FIG. 1. Data from high symmetry directions with $E_\gamma=55$ eV (a) Image of the spectral function along the Γ to (π, π) direction. (b) EDCs from (a). (c) Image of the spectral function along the $(\pi, -\pi)$ to (π, π) direction. (d) EDCs from (c). The lower piece of the parabola in (c) is slightly distorted from its intrinsic shape as these data were at the edge of the detector multichannel plate and were likely affected by astigmatism in the electron lens.

direction indicates a weaker electron-phonon interaction in $\text{Nd}_{1.85}\text{Ce}_{0.15}\text{CuO}_4$. A comparison along the $(\pi, 0)$ to (π, π) direction is more difficult for two reasons. The deviation from the Kramers-Kronig relation in the *n*-type sample is more serious, and the situation in *p*-type material is more uncertain.

II. EXPERIMENT

Angle-resolved photoemission data were recorded at beamline 10.0.1.1 of the Advanced Light Source with a photon energy of 55 eV in a glancing incidence geometry. Polarization angles were 45° to the Cu-O bonds for the Γ to (π, π) cut and along the Cu-O bonds for the $(\pi, 0)$ to (π, π) cut. Energy resolution was typically 18 meV and angular resolution was 0.14° (corresponding to $\approx 0.5\%$ of the Brillouin zone size). This is an identical configuration to that used in an extensive study of the kink in the hole doped compounds [8]. Samples were cleaved *in situ* at low temperatures in vacuum better than 4×10^{-11} Torr. As there are only minor changes to the spectra when entering the superconducting state [16], all displayed spectra were taken at low temperature ($\approx 15 - 25$ K) [16]. No signs of surface aging were seen for the duration of the experiment (≈ 24 h.). In addition to the displayed data, a large number of measurements were performed on beamline 5-4 of the Stanford Synchrotron Radiation Laboratory; results were obtained that are consistent with those displayed here.

Single crystals of $\text{Nd}_{1.85}\text{Ce}_{0.15}\text{CuO}_4$ were grown by the traveling-solvent grown method in 4 atm. of O_2 . The as-grown boules are not superconducting and must be annealed to remove excess apical oxygen. The displayed data comes from samples that were heated in flowing argon gas for 20 h. at 920°C and then a further 20 h. at 500°C under pure O_2 [18]. Resistivity and magnetic

susceptibility measurements show an onset of the superconducting transition at 24 K.

III. RESULTS

In Fig. 1, we show the raw data in the form of 2D false intensity plots of the spectral function, along with the corresponding EDCs for \vec{k} -space cuts, along the Γ to (π, π) and the $(\pi, 0)$ to (π, π) directions. In Fig. 2, we show the data represented in a more traditional fashion with EDCs selected at larger angular intervals (0.5°). In the Γ to (π, π) direction, a large broad feature disperses out of the background and sharpens to a peak at E_F and then disappears. As pointed out previously [15], this is behavior not unlike that found in optimally doped *p*-type compounds. A closer look below will reveal important differences. In the $(\pi, 0)$ to (π, π) direction an almost parabolic shaped band is seen. A similar sharpening of the feature as it disperses to E_F is seen here as well, however the EDCs seem to show additional structure in the form of two separate peaks. This aspect has been noted previously [15–17].

The MDCs from the raw false intensity plots in Fig. 1a and 1c were fitted to Lorentzians, as detailed above. Sample fits are shown in Fig. 3 at representative slices $\omega = 0$ and $\omega = 150$ meV. At energies higher than those displayed, the MDC lineshape begins to differ more significantly from a simple Lorentzian.

At the displayed relevant lower energies the MDCs fit the Lorentzian functional forms relatively well, showing that, although there may be large momentum dependence in the self-energy in other parts of the BZ, the changes across the displayed regions are minimal at low energy. The fact that the fits begin to break down at higher energies shows that momentum dependent effects may be coming into play. These position fits are dis-

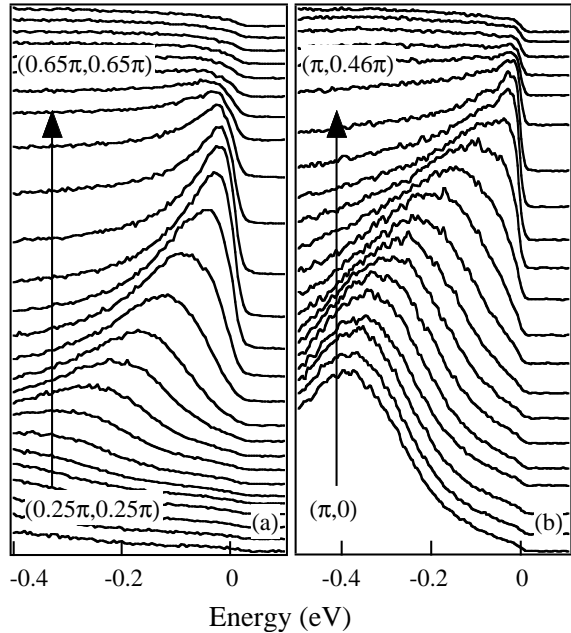


FIG. 2. $E_\gamma=55$ eV EDCs representing the data in a more traditional fashion. (a) $(0.25\pi, 0.25\pi) \rightarrow (0.65\pi, 0.65\pi)$. (b) $(\pi, 0) \rightarrow (\pi, 0.46\pi)$. The EDCs are shifted by an arbitrary offset.

played in Fig. 4 with the corresponding energy widths in Fig. 5. In Fig 4a we show the dispersion along the zone diagonal plotted from the momentum space peak position. As seen by comparison with the linear fit, there is only a gentle slope change of the dispersion and no sign of a sharp mass-renormalization at low energy. This is in sharp contrast to the *p*-type materials where this is the region of the BZ that shows the most unambiguous effect at ≈ 70 meV.

The behavior along the $(\pi, 0)$ - (π, π) direction differs from that of the zone diagonal. Here the smooth dispersion deviates at low energy from the parabolic fit in the region indicated by the arrow in Fig 4b. One sees that along the $(\pi, 0)$ - (π, π) cut there may be a small mass renormalization around 55 meV. This is the same energy scale where one sees a dip structure in the EDC in Fig. 2. This is the same energy scale as the mass renormalization onset in the *p*-type compounds. If one is to identify this apparent mass change with coupling to a bosonic mode, a simple analysis for the dimensionless coupling parameter with $\lambda' = \frac{\vec{v}_F^0}{v_F} - 1$ gives a value $\lambda' \approx 0.3$. This may be compared with values ≈ 0.5 extracted *via* the same method from the zone diagonal direction of the *p*-type materials near optimal doping. Note that there are some uncertainties in the quantitative estimate for λ' that deserve mentioning. The value for λ' is in actuality an upper bound on the full renormalization as there is no independent measure of the bare dispersion to get \vec{v}_F^0 . In this simple analysis we used as a value for \vec{v}_F^0 the \vec{v} from the dispersion above the expected kink energy and the

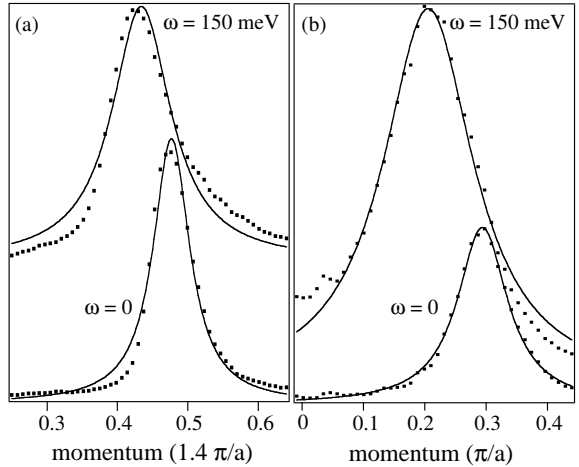


FIG. 3. MDCs from Fig. 1 at $\omega = 0$ and $\omega = 150$ meV binding energy along the two main symmetry directions. (a) $\Gamma \rightarrow (\pi, \pi)$ (b) $(\pi, 0) \rightarrow (\pi, \pi)$. Spectra are shifted by an arbitrary offset.

\vec{v}_F from a low ω fit, as was done in the analysis for the *p*-type materials [8].

Closer to the spirit of how a mass renormalization is typically defined would be to use a $\omega \rightarrow 0$ extrapolation of a function fitted to the dispersion at higher energy ($\omega > 100$ meV). Analyzing in this way gives velocities of $\vec{v}_F^{0eff}(\omega \rightarrow 0) = 4.3 \times 10^5$ m/sec (2.3 eV \cdot a \cdot $\hbar\pi$) for the Γ - (π, π) FS crossing and $\vec{v}_F^{0eff}(\omega \rightarrow 0) = 3.4 \times 10^5$ m/sec (1.8 eV \cdot a \cdot $\hbar\pi$) for the $(\pi, 0)$ - (π, π) FS crossing. Using this value for the $(\pi, 0)$ - (π, π) cut gives a smaller λ' of ≈ 0.1 . However, the values for λ' near $(\pi, 0)$ arrived at in this fashion are not readily comparable to the hole doped compounds along the zone diagonal as their dispersion there does not appear to recover asymptotically to something resembling an unrenormalized dispersion. This is most likely a consequence of the fact that for straightforward bosonic coupling one expects that the dispersion recovers to the bare one within about 5 times the bosonic band width. In the $(\pi, 0)$ region of the BZ the local electronic band width may be narrower than this bosonic bound, so one has to regain a parabolic dispersion more quickly. Curiously enough, a comparison of band structure calculations for similar cuprates to this $\omega \rightarrow 0$ extrapolated fit to the higher energy dispersion gives the calculated bare band velocity (2.2×10^5 m/sec) [19] to be lower than the experimental values. Given that both electron-electron and electron-boson interactions will enhance the effective mass and hence decrease the velocity, the fact that the measured velocity is higher than the band structure value may signal unexpected physics, or may be a red flag for the data analysis procedure, an issue we will come back to later.

We note that finite resolution effects should not cause an inaccurate parameterization except very close to the Fermi energy. Close to E_F where the Fermi function

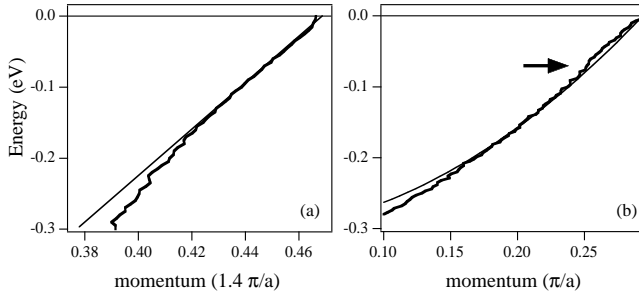


FIG. 4. Dispersions fitted from the spectral function analysis. (a) $\Gamma\rightarrow(\pi,\pi)$. The sharp upturn at low energies ($\omega < 15$ meV) is believed to be an artifact of the finite energy resolution. (b) $(\pi,0)\rightarrow(\pi,\pi)$. The smooth lines are simple fits (linear and parabolic for (a) and (b) respectively).

differs significantly from unity, finite energy resolution (ΔE) weights each individual ω point disproportionately towards higher energy so that only fits to ω higher than ΔE are reliable and intrinsic. The sharp change to higher velocity and steep drop in the scattering rate at $\omega < 15$ meV in the Γ to (π,π) direction are artifacts due to effects of this kind.

As detailed above, the widths of the MDC Lorentzians can be parameterized as $\Sigma''(\vec{k}, \omega)/\vec{v}_F^0$. As may be done for the case of λ' , in the absence of a definitive independent measure for \vec{v}_F^0 , we use as a $\vec{v}_F^{0\text{eff}}$ the \vec{v} from a $\omega \rightarrow 0$ extrapolation of a fit to a higher energy range to get a rough estimate for Σ'' . For instance in the $(\pi,0)\rightarrow(\pi,\pi)$ direction we use the value for the \vec{v}_F^0 of the fitted parabola. This fit, although displayed as extrapolated to $\omega = 0$, does not use input data for $\omega < 100$ meV. In Fig. 5 are shown the experimentally arrived at values for Σ'' .

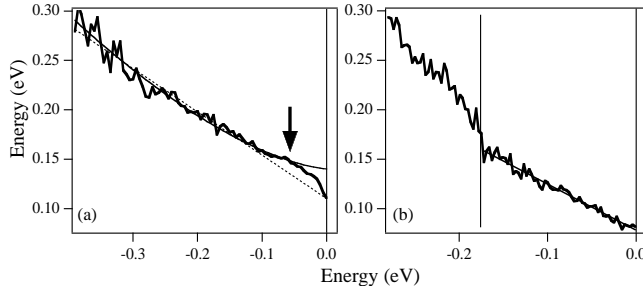


FIG. 5. Energy widths as fitted from spectral function MDCs and multiplied by velocity. (a) $\Gamma\rightarrow(\pi,\pi)$ The solid line and dashed line are power law fits $\Sigma''(\omega) = \Sigma''(0) + A\omega^\alpha$ with $\alpha = 1.55$ and 1 respectively. The arrow marks the point of low energy drop in Σ'' . (b) $(\pi,0)\rightarrow(\pi,\pi)$. The solid line is a linear fit. The vertical bar at 0.18 eV marks the energy region beyond which the MDC width fits are not reliable.

Along the $\Gamma\rightarrow(\pi,\pi)$ direction (Fig. 5a) $\Sigma''(\omega)$ is best fit (solid line) in the higher energy region (0.4 eV $> \omega > 0.09$ eV) to a power law of $\Sigma''(\omega) = \Sigma''(0) + A\omega^\alpha$ form with $\Sigma''(0) = 0.14$ eV and $\alpha = 1.55$. Note, that the best fit to a linear dependence (dashed line) with a finite $\Sigma''(0)$ of

0.11 eV does not fit nearly as well. There is a low energy drop in Σ'' at approximately 0.07 eV. Although the drop is subtle, we believe the effect to be intrinsic as it was seen in a number of samples. Note that this is close to the same energy that the mass renormalization is found at in the $(\pi,0)\rightarrow(\pi,\pi)$ direction. The precipitous drop in Σ'' for $\omega < 15$ meV, again, appears to be an artifact of finite energy resolution.

In contrast, along the $(\pi,0)\rightarrow(\pi,\pi)$ direction $\Sigma''(\omega)$ is best fit by a linear dependence on ω with $\Sigma''(0) = 0.08$ eV with no signature of a low ω drop in the scattering rate. Note that due to the much smaller local electronic bandwidth in this region of the BZ, the MDC Lorentzian fit breaks down at energies higher than ≈ 0.2 eV as may have been expected from a visual inspection of Fig. 1c. It is interesting to note that $\Sigma''(0)$, extracted in this way, is very different for the two directions. Also note that the finite energy (ΔE) and momentum resolution ($\Delta \vec{k}$) only give a minor broadening contribution to Σ'' as $\Delta \Sigma'' = \sqrt{(\partial E_{\vec{k}}/\partial \vec{k} \cdot \Delta \vec{k})^2 + (\Delta E)^2} \approx 28$ meV.

IV. DISCUSSION

As discussed above and in Ref. [8], due to its ubiquity, temperature dependence, and energy scale, the strong velocity renormalizations in the p -type materials may be reasonably attributed to an interaction of the charge-carriers with phononic degrees of freedom. In the n -type compounds we see some evidence of possibly similar effects although important differences exist. As detailed above, there is no kink along the zone diagonal, which is the region of the BZ that shows the most unambiguous effect in the hole doped materials. There does appear to be a kink along the $(\pi,0)$ to (π,π) direction, however as we will discuss below, the interpretation is not as straightforward.

If there are effects due to the fluctuations of some kind of symmetry reducing order with characteristic wave vector (π, π) then one may expect to see two features in the EDCs in portions of the BZ where the Fermi sea is occupied in momentum regions straddling both sides of the AFBZ boundary. For instance EDCs from near the Fermi surface near $(\pi, 0.3\pi)$, may have features from the unreconstructed bands well below E_F from near $(0, 0.7\pi)$. In contrast EDCs from the band near $(0.45\pi, 0.45\pi)$ will not have features from near $(0.55\pi, 0.55\pi)$ as this is well above E_F . In this way such a BZ reducing order may be expected to greatly modify the spectral function near $(\pi, 0)$, but not as much near $(\pi/2, \pi/2)$ for an unreconstructed hole-like Fermi surface centered at (π, π) . Two such features in the EDC can give a kink in the effective dispersion if an MDC analysis, as detailed above, is performed. As it has been previously noted that there are two features in the EDCs near the $(\pi, 0)$ position

[15–17] (see Fig. 2b) and there is evidence for fluctuations of some kind of (π, π) symmetry reducing order, we do not feel that there is sufficient evidence to assign this kink feature, found by an MDC analysis, the same origin as the kink observed in the *p*-type compounds. We believe there is no way to unambiguously separate the (π, π) symmetry reducing effect. One the other hand, this (π, π) scattering, which, if associated with spin fluctuations, is broad in energy and presumably has an energy spectrum which changes with doping [20]. It seems improbable that this $(\pi, 0)$ to (π, π) kink will occur at a particular energy so close to relevant phonons. A doping dependent study may clarify these issues; if the 55 meV scale changes with doping, then it is likely of lattice origin.

However, one can make a strong statement about the lack of a kink along the zone diagonal. By the same condition given above, in this region of the BZ we do not expect to see (π, π) features (nor are any observed) as the Fermi sea is only filled on one side of AFBZ boundary. Visual inspection of the MDC fitted dispersion in the $0.2 \text{ eV} > \omega > 0 \text{ eV}$ range shows there is a slight negative curvature that may be due to ordinary band effects or electron-electron interactions, but there is no feature resembling a sharp kink.

The dependence of the scattering rate on frequency along the zone diagonal is different than the linear dependence reported in the optimally doped *p*-type materials [21] (however, note that other groups have found possible deviations from linear [22]). This stronger $\omega^{1.55}$ dependence in the electron doped compounds may be compared to the quadratic temperature dependence of their resistivity vs. the linear dependence of the hole doped materials [23,24].

A number of groups have found a linear dependence of the low-energy ($>1000 \text{ cm}^{-1}$) scattering rate by an inversion of the optical conductivity [25,26]. As the conventional wisdom is that zone diagonal states give the primary contribution to transport due to their higher \vec{v}_F , this at first glance is not consistent with our finding here. However, as we have found for the present material that the \vec{v}_F at the Γ - (π, π) FS crossing is not greatly different from that found at the $(\pi, 0)$ - (π, π) FS crossing [i.e. the $(\pi, 0)$ saddle point is $\approx 300 \text{ meV}$ below E_F] the $(\pi, 0)$ region (where a linear dependence is found) may contribute somewhat equally to the optical scattering rate. Moreover, as may be seen in Fig. 5a the scattering rate along the zone diagonal can be fit approximately by a linear dependence above 130 meV and it may be that it is this energy which is contributing the most to the optical excitations for $E_\gamma > 1000 \text{ cm}^{-1}$ ($\approx 100 \text{ meV}$). Optical experiments also find a low energy drop in the scattering rate below an energy ($650 \text{ cm}^{-1} \approx 70 \text{ meV}$) very close to where we find the depression in Σ'' and mass renormalization [25,26].

The energy at which we observe the mass renormal-

ization along the $(\pi, 0)$ to (π, π) direction is the same energy to within experimental uncertainty that we observe the drop in the scattering rate along the zone diagonal. We should point out that although these energy scales are consistent with each other, this observation is inconsistent with Kramers-Kronig considerations. As Σ' and Σ'' are real and imaginary components derived from the same response function, they should be related *via* a Kramers-Kronig transform due to causality. If Σ' along a particular cut shows a kink, then Σ'' should show a corresponding drop. The reason such a behavior is not observed is unclear, but may be related to momentum dependence in the self-energy masking the effect. If the self-energy is momentum dependent the dispersion and width obtained from MDC analysis cannot be simply related to Σ' and Σ'' respectively. This cautions any quantitative result that one extracts from this type of analysis. However, it does seem that the qualitative conclusion that there is little renormalization along the zone diagonal will likely remain valid. The situation for the $(\pi, 0)$ - (π, π) direction is less clear, as the mass renormalization is stronger here and the situation in the *p*-types near $(\pi, 0)$ more uncertain.

As detailed above, it seems reasonable to associate the mass renormalization on the *p*-type side of the phase diagram with a strong coupling of charge carriers to phononic degrees of freedom. Specifically, the phonon has been conjectured [8] to be the oxygen half-breathing mode, which is seen to have anomalous softening and spectral weight changes in the relevant energy range near the doping induced metal-insulator transition as probed by neutron scattering [27–30].

A number of recent studies have found similar signatures of phononic anomalies in the electron doped materials [31,32]. Kang *et al.* found the growth of new lattice modes in the generalized phonon density of states around $\approx 70 \text{ meV}$ by neutron scattering. d’Astuto *et al.* measured phonon dispersions *via* inelastic x-ray scattering and assigned the softening and growth of new lattice modes they found in the 55 - 75 meV energy range to the same oxygen half-breathing mode that anomalies are found in the *p*-type materials. These studies give evidence for phononic effects in the electron doped materials that are somewhat similar to those found in the holed doped compounds.

However, there are a number of differences that exist in these anomalies between the two sides of the phase diagram which may provide a starting point to understanding why similar signatures may not appear in the ARPES spectra. Although the biggest changes in the phonon density of states probed by Kang *et al.* happen at similar doping levels in $\text{La}_{2-x}\text{Sr}_x\text{CuO}_4$ and $\text{Nd}_{2-x}\text{Ce}_x\text{CuO}_4$ ($x \approx 0.04$), the dopings levels are at very different relative positions in the phase diagram, with $x = 0.04$ being still well into the antiferromagnetic (and possibly more insulating) phase for the electron doped com-

ound. As such modifications in the phonon spectrum may be associated generally with screening changes (and hence electron-phonon coupling) with the onset of metallicity, this demonstrates the possibility that the changes in the NCCO phonon spectrum, although being superficially similar in the electron and hole doped materials, are in some sense different. d'Astuto *et al.* found that although the softening of the phonon dispersion appears in a somewhat similar way at a similar energy scale as in the *p*-types, differences do exist in the shape of the anomaly in the phonon dispersion.

On general grounds, since the probed soft phonon is the oxygen half-breathing mode, one may naively expect a weaker coupling for this mode with electron doping, as Madelung potential considerations [33] give that doped electrons will preferentially sit on the Cu site, whereas doped holes are primarily weighted on oxygen.

Although Kang *et al.* have mentioned [31] that it would be interesting to look for mass renormalizations in the *n*-type underdoped compounds where they first detect phonon anomalies, we feel that if the electron-phonon coupling is of the same nature in the *n*- and *p*-type materials it should show up in the ARPES spectra of the highest- T_c electron doped samples as it does in the hole doped. Moreover, the issue of looking for mass renormalizations and at peak widths may not even be relevant at the extremely low dopings ($x = 0.04$) where Kang *et al.* see the largest changes, as there are only regions of the BZ with enhanced near- E_F spectral weight and no well defined electronic peaks [34]. In fact, the question of what the electron-phonon coupling is as one enters the Mott insulating state at very low dopings, may not be particularly well posed, as the near- E_F spectral weight vanishes as $x = 0$ is approached. The Mott effect may make these other effects harder to detect.

V. CONCLUSION

A modern spectral function analysis reveals very different and likely weaker signatures of possible bosonic effects in the ARPES spectra of $\text{Nd}_{1.85}\text{Ce}_{0.15}\text{CuO}_4$ along the two main symmetry directions of the BZ. However, unlike the *p*-type compounds we believe that one cannot distinguish the various contributions to the self-energy into separate effects, as the simple analysis yields results which are not consistent with Kramers-Kronig considerations. Despite the complexities inherent in assigning various features in the spectra to distinct sources, a direct comparison between the *p*- and *n*-types compounds does have utility, as we have shown the lack of a mass renormalization along the zone diagonal. Our analysis shows that whatever is causing the distinct effect in the hole doped materials manifests itself weaker on the *n*-type side, either due to a weaker electron-phonon coupling or due to masking effects from other interactions.

Such an observations is consistent with a weaker electron-phonon coupling in the electron doped cuprates, however a strong discrepancy exists between these measurements and a number of scattering studies that point to strong electron-phonon coupling. Perhaps, some of the intrinsic differences between electron and hole doping may provide a route towards reconciling these different measurements and thereby giving insight into the underlying phenomenon.

VI. ACKNOWLEDGMENTS

The authors would like to thank J.D. Denlinger for access to his data analysis routines and M. d'Astuto, A. Lanzara, and S.A. Kivelson for helpful conversations. Experimental data were recorded at the Advanced Light Source which is supported by the DOE Office of Basic Energy Science, Division of Materials Science with contract DE-AC0376SF00098. Additional support was through the Stanford Synchrotron Radiation Laboratory which is operated by the DOE Office of Basic Energy Science, Division of Chemical Sciences and Material Sciences. The Stanford crystal growth was supported by the U.S. Department of Energy under contracts No. DE-FG03-99ER45773 and No. DE-AC03-76SF00515, by NSF CAREER Award No. DMR-9985067, and by the A.P. Sloan Foundation. The crystal growth work in Tokyo was supported in part by Grant-in-Aids for Scientific Research from the Ministry of Education, Science, Sports, and Culture, Japan, and NEDO.

- [1] A. Damascelli, Z.-X. Shen, and Z. Hussain, *Rev. Mod. Phys.* **75**, XXXXX (2003).
- [2] S. Hüfner, *Photoelectron spectroscopy: Principles and Application*, New York: Springer-Verlag (1995).
- [3] C.M. Varma *et al.*, *Phys. Rev. Lett.* **63**, 2602 (1989).
- [4] M. Hengsberger *et al.*, *Phys. Rev. Lett.* **83**, 592 (1999).
- [5] S. Lashell, E. Jensen, and T. Balasubramanian, *Phys. Rev. B* **61**, 2371 (2000).
- [6] T. Valla *et al.*, *Phys. Rev. Lett.* **83**, 2085 (1999).
- [7] P.V. Bogdanov *et al.*, *Phys. Rev. Lett.* **85**, 2581 (2000).
- [8] A. Lanzara *et al.*, *Nature* **412**, 510 (2001).
- [9] A. Kaminski *et al.*, *Phys. Rev. Lett.* **86**, 1070 (2001).
- [10] P.D. Johnson *et al.*, *Phys. Rev. Lett.* **87**, 177007 (2001).
- [11] A.D. Gromko *et al.*, cond-mat/0202329.
- [12] Hae-Young Kee, Steven A. Kivelson, and G. Aeppli, *Phys. Rev. Lett.* **88**, 257002 (2002).
- [13] See for instance S. Chakravarty *et al.*, *Phys. Rev. B* **63**, 094503 (2001).
- [14] Y. Tokura, H. Takagi, and S. Uchida, *Nature* **337**, 345-347 (1989).
- [15] N.P. Armitage *et al.*, *Phys. Rev. Lett.* **87**, 147003 (2001).

- [16] N.P. Armitage *et al.*, Phys. Rev. Lett. **86**, 1126 (2001).
- [17] T. Sato, T. Kamiyama, T. Takahashi, K. Kurahashi, and K. Yamada, Science **291**, 1517-19 (2001).
- [18] Data consistent with those presented here were also obtained on samples where the reducing condition was 100 hours in flowing argon gas at 1000 C.
- [19] P. B. Allen, W. B. Pickett, and H. Krakauer, Phys. Rev. B **36**, 3926 (1987).
- [20] K. Yamada *et al.*, cond-mat/0210536.
- [21] T. Valla *et al.*, Science **285**, 2110 (1999).
- [22] X.J. Zhou *et al.*, *in preparation*.
- [23] F. Gollnik and M. Naito, Phys. Rev. B **58**, 11734 (1998).
- [24] Y. Onose, and Y. Taguchi, K. Ishizaka, and Y. Tokura, Phys. Rev. Lett. **87**, 217001 (2001).
- [25] C.C. Homes *et al.*, Phys. Rev. B **56**, 5525 (1997).
- [26] E.J. Singley, D.N. Basov, K. Kurahashi, T. Uefuji, and K. Yamada, Phys. Rev. B **64**, 224503 (2001).
- [27] R.J. McQueeney *et al.*, Phys. Rev. Lett. **82**, 628 (1999).
- [28] R.J. McQueeney *et al.*, Phys. Rev. Lett. **87**, 077001 (2001).
- [29] L. Pintschovius and M. Braden, Phys. Rev. B **60**, R15039 (1999).
- [30] Y. Petrov *et al.*, cond-mat/0003414.
- [31] H.J. Kang *et al.*, Phys. Rev. B **66**, 064506 (1999).
- [32] M. d'Astuto *et al.*, Phys. Rev. Lett. **88**, 167002 (2002).
- [33] J. B. Torrance and R. M. Metzger, Phys. Rev. Lett. **63**, 1515 (1989).
- [34] N.P. Armitage *et al.*, Phys. Rev. Lett. **88**, 257001 (2002).